Synthetic jet modeling for U-RANS

By F. Capizzano† AND G. Iaccarino

This work focuses on different approaches for the numerical simulation of a Synthetic Jet device via RANS codes. The objective is to explore possible RANS techniques to utilize in a more general design loop with flow control purposes. A turbulent flow over a hump model with a contoured slot in three different working conditions (no-flow control, steady suction and oscillatory control) is considered for our validation tests. The device itself is not simulated but its effects are modeled using specially designed boundary conditions (BC). Comparisons of numerical results obtained with various BC formulations and experimental data are carried out.

In the second part of the paper a preliminary study of a lumped model in which the time averaged flow field is resolved using a steady state approach is presented. A source term is added in the momentum equation to account for the unsteadiness generated by the pulsating jet. The source term is related to a scalar quantity whose field is governed by a classical convection-diffusion type transport equation.

1. Introduction

The study of devices for controlling the boundary layer characteristics is receiving renewed interest due to the introduction of a new family of piezoelectric actuators named Synthetic Jets (SJ). They consist of a deforming membrane oscillating into a close cavity. A periodic suction/blowing flow is established at its small exit orifice. SJs add momentum into the external boundary layer like classical continuous jets but have the advantages of requiring low electrical power supply and no piping. A good review of SJ applications along with unresolved questions has been given by Kral *et al.* (1997).

Computational fluid dynamics is currently heavily used to investigate both the basic operating principles of SJs; in the near future fast, reliable prediction tools based on CFD will be required to design control systems based on these devices. Direct numerical simulations and large eddy simulations have been performed with good results (Catalano *et al.* 2002; Conrad *et al* 2002; Rumsey *et al.* 2004). These simulations, though of key interest for the understanding of complicated interactions between an external cross flow and a single SJ, require massive resources and are too time consuming when used to answer to practical aerodynamic design questions (such as the number and positions of the actuators over a wing). On the contrary Reynolds-Averaged Navier-Stokes (RANS) simulations offer sufficient predicting performances with relative low computational costs. In this paper, we are interested in evaluating the feasibility and the accuracy of RANS modeling for the simulation of turbulent flows controlled by synthetic jets. Recently a workshop (CFDVAL2004) on numerical simulation of synthetic jets and turbulent separation control was held under joint sponsorship by NASA and ERCOFTAC. Results collected in Rumsey *et al.* (2004) illustrate the substantial equivalence between BC models and direct simulation of the cavity (plenum) flow. This was partly due to the inherent difficult characterization of the membrane motion that introduces uncertainties. Another

† CIRA Italian Aerospace Research Center, Via Maiorise 81043 Capua (CE), Italy

interesting question raised at the workshop was: is it possible to capture the unsteady effects of a SJ in an external boundary layer as a steady problem?

In previous works such as Kral *et al.* (1997) and Iaccarino *et al.* (2003), RANS modeling coupled with specific boundary conditions is preferred to an explicit simulation of the jet cavity. Several contributors in the CFDVAL2004 workshop used BC models especially for the hump model case (separation control). This case has been studied experimentally in the NASA Langley Transonic Cryogenic Tunnel with CFD validation in mind. A low mach number $2D$ flow ($Mach = 0.1$) passes over a hump wall; in the recovery region a slot exit is applied to control the natural separation bubble. The first part of the paper deals with steady/unsteady simulations in which an appropriate boundary condition model is applied at the slot exit.

The objective of the second part of our research project was to investigate the feasibility of a lumped model to approximate synthetic jets in the context of steady-state RANS simulations. The rationale is that synthetic jets inject momentum in the external flow but do not add mass (as opposed to conventional active control devices based on blowing). This implies that, if we solve the steady-state governing equations with suitable forcing terms in the momentum equations, we will be able to duplicate the time-average effect of an oscillating jet. The idea of unsteady phenomena modeled as a body force go back to Lighthill acoustic streaming theory. Recently Riley (2001) developed a theory for an oscillatory nonconservative body force in homogeneous fluids. Pes *et al.* (2002) add, in the momentum equation, a source term containing information about unsteady characteristics of the SJ/crossflow interactions. They evaluate the source term using a deterministic neural-network based code. The real difficulty is related to the evaluation of the source term. The method proposed here links the source term to a scalar field containing information about SJ characteristic parameters identified by experimentalists, Glezer & Amitay (2002), Smith *et al.* (2003) (e.g. the stroke length L_0 and the impulse associated with the discharge phase I_0). An expression for the source term is proposed along with the scalar field transport equation and the relative boundary condition.

2. Numerical method

The numerical analysis presented here has been carried out using the CIRA U-ZEN multi-zone flow solver(Catalano *et al.* 2003). It is a multiblock structured grid code able to solve steady and unsteady compressible Reynolds-Averaged Navier-Stokes equations around complex $3D$ geometries. A cell-centered finite volume approach with Jameson-type artificial dissipation is used as a discretization technique for the equations in conservation form. A steady state solution is obtained using an iterative multistage Runge-Kutta scheme which is accelerated using a local time stepping process and an implicit residual averaging. Geometric multigrid based on the the RK scheme is used to accelerate the convergence to steady state. Time-accurate solutions are obtained using a dual time stepping method. Several eddy viscosity turbulence models are available in U-ZEN including non linear models. All the numerical tests have been performed assuming a fully turbulent $2D$ incompressible flow ($Mach = 0.1$) using Myong & Kasagi (1990) $\kappa - \epsilon$ and the Menter (1994) SST $\kappa - \omega$ as closure models. Some modifications have been introduced in the original version of U-ZEN for a correct integration of SJ boundary condition models.

3. Boundary condition model

In this section the boundary condition models adopted for the steady and unsteady simulations are discussed. Hereafter a non-dimensional formulation is considered based on the free-stream flow quantities and the hump chord, c. As outlined above, the SJ effect on the external boundary layer is modeled by a space and time dependent jet-velocity distribution

$$\mathbf{u} = \mathbf{U}_J(\xi, \eta, t) \tag{3.1}$$

where (ξ, η) is a curvilinear reference system along an imaginary line leveled with the hump surface and $\mathbf{U}_J = U_{Jn}\widehat{\eta} + U_{Jt}\widehat{\xi}$.

3.1. *Steady model*

For a steady blowing/suction control analysis, the coefficients of mass and momentum at the slot exit are considered

$$C_{\dot{m}} = \rho_J U_{Jn} h \tag{3.2}$$

$$C_\mu = 2\rho_J U_J^2 h \tag{3.3}$$

respectively, where $\rho_J = \rho_J^*/\rho_\infty = 1$, $U_J = U_J^*/U_\infty$ and $h = h^*/c$ are the non-dimensional jet density, velocity and slot width. The first option to model $\mathbf{U}_J(\xi, \eta, t)$ is a top-hat velocity distribution based on the integral information $C_{\dot{m}}$

$$\text{1st model} \quad \begin{cases} U_{Jn} = C_{\dot{m}}/\rho_j/h \\[2mm] \mathbf{u}(\xi) = U_{Jn}\widehat{\eta} \end{cases} \tag{3.4}$$

In this case C_μ is not directly used but rather verified *a posteriori*. A similar BC was chosen by Viken *et al.* (2003) for their numerical tests. Their results show discrepancies in the pressure recovery region between numerical and experimental data as for suction and blowing. As pointed out by the authors many factors, such as the BC model deficiencies, turbulence model and $3D$ effects during experiments, play a role. Analogous discrepancies were found by Iaccarino *et al.* (2003) who also compared numerical solutions with and without cavity flow. A second option, as described by Marongiu *et al.* (2004), is to take advantage of both integral information $C_{\dot{m}}$ and C_μ to introduce a tangential component U_{Jt} at the slot exit

$$\text{2nd model} \quad \begin{cases} U_{Jn} = C_{\dot{m}}/\rho_j/h \\[2mm] U_{Jt} = U_{Jn}\tan(\theta) \\[2mm] \tan(\theta) = \sqrt{C_\mu/(2U_{Jn}^2 h)} \\[2mm] \mathbf{u}(\xi) = U_{Jn}\widehat{\eta} + U_{Jt}\widehat{\xi} \end{cases} \tag{3.5}$$

Top-hat velocity distributions used in the above two models are poor approximations of the complex flow near the orifice. A further BC model uses a spatially varying velocity distribution at the SJ cavity, using zero gradient extrapolation from the domain interior. During the iterative process, to ensure the correct integral mass flow rate, the following

procedure is used

$$
\text{3rd model} \quad
\begin{cases}
U_{Jn} = C_{\dot{m}}/h \\[2mm]
\frac{\partial}{\partial \eta}\mathbf{u}(\xi) = 0 \implies \mathbf{u}(\xi)|_{extrapol.} \\[2mm]
\triangle\mathbf{u}(\xi) = U_{Jn}\widehat{\xi} - \mathbf{u}(\xi)|_{extrapol.} \\[2mm]
\mathbf{u}(\xi) = \mathbf{u}(\xi)|_{extrapol.} + \triangle\mathbf{u}(\xi)
\end{cases}
\tag{3.6}
$$

The procedure based on (3.6) is physically correct in the case of suction but it does not satisfy the characteristics of blowing because no information, except for the pressure field, can be extrapolated from inside the domain. A revised procedure (3.6) for blowing starts from the following extrapolation:

$$
\frac{\partial}{\partial \eta}p(\xi) = 0 \implies p(\xi)|_{extrapol.}
\tag{3.7}
$$

A fully developed incompressible laminar flow coming from the slot duct can be assumed and a pressure-corrected velocity distribution, on center line, is derived as

$$
\text{blow correction} \quad
\begin{cases}
U_{Jn} = \sqrt{(2/3C_{\dot{m}}/h)^2 + 2(1 - p(\xi)|_{extrapol.})} \\[2mm]
\mathbf{u}(\xi) = U_{Jn}\widehat{\eta}
\end{cases}
\tag{3.8}
$$

This correction takes the place of $\frac{\partial}{\partial \eta}\mathbf{u}(\xi) = 0$ in the procedure (3.6).

An additional modification can be included to account for the exact geometrical shapes in proximity of the slot exit

A Neumann boundary condition on the orifice exit for the turbulent variables is enforced for each of the three models.

3.2. *Unsteady model*

During oscillatory suction/blowing, a zero net mass flux through the orifice is established:

$$
\frac{1}{T}\int_0^T \mathbf{u}(\xi,t)dt = 0
\tag{3.9}
$$

where $T = 1/f$ is the device forcing period.

Although there is no guarantee that this integral condition is satisfied locally each point on the orifice and given the limited experimental information for the spatial and temporal variations, we simply use the membrane forcing as the one-mode frequency:

$$
C_{\dot{m}}(t) = \rho_j h U_J^{max} sin(2\pi f t)
\tag{3.10}
$$

where f is the suction/blowing frequency and U_J^{max} is the peak velocity out of slot during blowing part of the cycle. The application of the three spatial model (3.4), (3.5) and (3.6), requires the instantaneous mass flux condition

$$
\frac{1}{h}\int_0^\xi \mathbf{u}(\xi,t)d\xi = C_{\dot{m}}(t)/\rho_j/h
\tag{3.11}
$$

Compared to the first and second models, this means a constant velocity distribution which remains self-similar when modulated by a certain time frequency. Otherwise when

the third model is applied, the resulting $\mathbf{u}(\xi)$ can change its spatial form during the temporal process, thus obtaining a new way of characterizing the expression (3.1).

As for steady simulations, a Neumann condition is assumed for the turbulent variables.

4. The hump model case

The configuration selected for the present study is a $2D$ channel flow with a bottom wall mounted Glauert-Goldschmied half-airfoil (Figs. 1 and 2). The non-dimensional domain based on the hump chord length ($c = 0.42m$) extends approximately $2c$ and $4c$ upstream and downstream of the hump respectively and $0.9c$ in the normal direction. A collection of experimental data are available for the steady cases (base-flow and steady suction) at a Reynolds and Mach number of $Re = 9.36 \times 10^5$ and $M_\infty = 0.1$ based on a free-stream velocity $U_\infty = 34.6m/s$. Two end-plates in the span-wise direction are used in the experiment to guarantee a nominal $2D$ flow in the center plane; they introduce a considerable blockage effect and, therefore, in the simulations a contoured shape of the top wall is introduced to mimic the acceleration introduced by the plates. In the no-flow control case a natural separation occurs near 65% of the chord followed by a reattachment near the $x/c = 1.11$ location. The resulting separation bubble extends $\Delta/c = 0.435$ approximately. A slot is introduced near 65% chord to control flow separation. Two computational single-block grids are built both counting 728×198 cells at the finest of three grid levels, having a first cell height $\Delta y/c$ of $1 \cdot 10^{-5}$; this leads to an acceptable resolution of the viscous sublayer ($y^+ \leq 0.5$). The two grids differ in the contouring of the upper wall shape. The cavity region is not meshed and the slot exit is discretized using 64 grid cells in the stream-wise direction with clustering near the corners. In Table 1 are summarized the boundary conditions adopted for the no flow-control case simulations. Experimental velocity u profile is prescribed at the inflow along with a turbulent kinetic energy (k) distribution derived by the available experimental turbulent stresses u'^2 using an empirical correlation to link the root-mean-squared turbulent velocities u', v' and w' (fully-developed turbulent boundary layer on a flat plate)

$$k = \frac{1}{2}(u'^2 + v'^2 + w'^2) \approx \frac{1}{2}[u'^2 + (\frac{1}{2}u')^2 + (\frac{3}{4}u')^2] = .90625. \cdot (u')^2 \qquad (4.1)$$

In Figs. 3 and 4, C_P and C_f distributions are compared using the two grids described above. The corrected top wall grid matches more closely the expansion peak and therefore the pressure plateau into the bubble. Hereafter we present only results obtained on the profiled upper wall grid. The C_P and C_f distributions, obtained with SST $\kappa - \omega$ and $\kappa - \epsilon$ closure models, are compared in Figs. 5 and 6. Both models produce acceptable expansion peak (at the beginning of the recovery region) and pressure level inside the bubble. On the contrary they over-predict the recirculation zone extension delaying the experimental reattachment point from $x/c \approx 1.11$ to $x/c = 1.62$, using $\kappa - \varepsilon$, and $x/c = 1.27$ using $\kappa - \omega$. Comparisons of stream-wise velocity (Figs.7 and 8) and turbulent kinetic energy (Figs.9 and 10) in two stations fore (65% chord) and aft (80% chord) the slot exit suggest a low level of turbulent shear stress. It is evident inside the bubble (Fig. 10) an under-prediction of the turbulent kinetic energy respect to the experimental data.

5. Separation control: results and discussions

Steady and unsteady separation control are analyzed in this section. A detailed experimental database is available for steady suction (CFDVAL2004) allowing a sufficient

TABLE 1. No-flow control case: boundary conditions

	u	v	p	κ
Inflow	experim.	0	experim.	experim.
Outflow	extrapol.	extrapol.	$p/p_\infty = 0.99944$	extrapol.
Upper − wall	slip	slip	extrapol.	κ_∞
Bottom − wall	no-slip	no-slip	extrapol.	0

calibration of the numerical boundary conditions. The experimental steady suction mass flow rate is $C_{\dot{m}} = 1.509 \cdot 10^{-3}$ reported to the slot exit width $h/c = 4.5 \times 10^{-3}$ at level with the hump surface. Three kinds of steady boundary condition are explored. Numerical tests, not reported here, show little difference between these three BC models in terms of Cp and Cf distributions. For brevity only the results obtained with the 3rd model are reported. Steady suction pressure coefficient (Fig. 11) shows an acceptable pressure level in the separation bubble but its extension is over-predicted compared to the experimental data. Skin friction comparison (Fig. 12) confirms this deficiency even if the bubble extension reduction ($\approx 25\%$) is of the same order of experimental one. Comparisons of stream-wise velocity and turbulent kinetic energy at two stations upstream (65% chord) and downstream (80% chord) the slot exit are shown in Figs. 13–16. As expected, the main reason for the over–predicted bubble extension is due to low mixing in the separated region (Fig. 16).

Unsteady computations are carried out applying the third BC model with the blow-phase correction (3.8). This one is less stiff in respect to top-hat BC models which impose singularities at the slot exit corners. Turbulence closure is obtained by Myong & Kasagi $\kappa - \varepsilon$ model. An experimental zero-net-mass-flux oscillatory suction/blowing frequency of $f = 138.5Hz$ is imposed. Peak velocity out of slot during blowing part of cycle is $U_J^{max} = 26.6m/s$. Its position is unknown. The non-dimensional forcing period is $T =_J^{max} /(fc) = 1/St = 0.5948$ (where St is the Strohual number) is divided into 720 time steps. To ensure periodicity, a number of 20 synthetic jet characteristic cycles are carried out. When periodicity is achieved a further cycle is run to average the flow field. A comparison between numerical and experimental mean Cp distribution, Fig. 17, shows a qualitative feasibility of the BC model in place of a complete SJ device simulation. The quality of the prediction (cfr. Figs. 18 and 19) can be improved using a different turbulence model, e.g. $SST\kappa - \omega$ model, as verified in the steady cases. In the Fig. 20, u and v velocity power spectra in two zones of the controlled boundary layer are reported: $x/c = 0.86$ (steady bubble zone), $x/c = 2.0$ (downstream reattachment point). The forcing frequency and its harmonics are clearly represented within the flow.

6. A preliminary study of a body force approach for a time averaged steady state simulation: a simple laminar case

Steady state approach to periodic unsteady phenomena has been formalized in the *steady streaming* theory for homogeneous fluids (Riley 2001). When an oscillating non-conservative forcing (of the form $sin(\omega t)$) is present in an incompressible flow field, fluctuating vorticity is generated inside the fluid. At leading order, the above vorticity field has non-zero time-average value. This concept is utilized by Pes *et al.* (2002) to approach

the problem of a synthetic jet from a steady point of view. They model synthetic jet unsteadiness using a neural network-based deterministic source term which is added to the right hand side of the momentum equations. However repeated unsteady computations are necessary to train the neural network based algorithm with different combination of the input parameters. Here an alternative way of obtaining the source term is illustrated. The basic idea is to use a scalar to describe the momentum transfer from the synthetic jet to the external flow. Experimental studies of Glezer & Amitay (2002) and Smith *et al.* (2003) of synthetic jet fluid mechanics in cross flow, identify characteristic length and velocity scales

$$L_0 = \int_0^{T/2} u_0(t) dt \tag{6.1}$$

$$U_0 = L_0 f = f \int_0^{T/2} u_0(t) dt \tag{6.2}$$

where $u_0(t)$ is the center line velocity averaged over the area of the orifice and $T = 1/f$ is the oscillation period. It is natural to relate the transported scalar to these quantities. One choice is the product of the oscillating frequency and the velocity scale U_0 (this quantity has the dimension of an acceleration, i.e. is appropriate as a momentum body force)

$$\phi = fU_0. \tag{6.3}$$

The value of this scalar quantity is known at the jet orifice and it is there prescribed as a boundary condition (note that the orifice is a no-slip boundary for the steady-state mean flow). The evolution of the scalar is governed by a convection/diffusion equation. The momentum transfer is described via a body force **F** on the basis of the scalar value and eventually its gradient

$$\mathbf{F} = L_0 \nabla \phi \tag{6.4}$$

In order to design the corresponding forcing terms, we performed few simulations of a synthetic jets in a time-accurate mode and then extracted, for each case, the "exact" forcing terms that would reproduce the time-averaged flow field. These forcing terms have been derived in terms of the most important design parameters for synthetic jets: frequency, maximum blowing velocity, cross-flow velocity and Reynolds number, etc. The configuration selected is a simple two-dimensional jet in a flat plate boundary layer. Initial work during the summer has focused on the construction of this database of time-accurate solutions. Preliminary results are very encouraging.

7. Future works

Unsteady RANS simulations have been carried out for flows with active flow control devices. The present results demonstrate a qualitative capability of modeling synthetic jets using simple boundary conditions. The details of the velocity distributions at the orifice exit do not seem to have a strong influence on the results. Turbulent variables of closure models are treated, at orifice, with a zero gradient conditions: more sophisticated conditions will be explored in the future.

A preliminary work has been carried out to develop a scalar transport equation for the modeling synthetic jets in a steady-state fashion. The major advantage of this approach is that once the tuning is completed, the present procedure can be implemented in a close-form within any CFD code. If it is successful, the proposed model would be substantially

faster than conventional time-dependent methods to study these control devices, and would make design and optimization of active flow control systems affordable.

8. Acknowledgments

The authors wish to thank Dr. N. Mansour at NASA Ames, and Prof. Paul Durbin at Stanford University, for the helpful discussions during the summer program and Dr. D. You for reviewing the manuscript.

REFERENCES

CATALANO, P., WANG, M., IACCARINO, G., SBALZARINI, L. & KOUMOUTSAHOS, P. 2002 Optimization of cylinder flow control via actuators with zero–mass flux. *Proc. of 2002 Summer Program*, Center for Turbulent Research, 297–304.

CATALANO, P., AMATO, M. 2003 An evaluation of RANS turbulence modeling for aerodynamic applications. *Aerospace science and Technology*, 7-7, 493–590.

CONRAD, Y. L. & GOLDSTEIN, D.B. 2002 Two-dimensional synthetic jet simulation. *AIAA J.* **40**, 510–516.

GLEZER, A. & AMITAY, M. 2002 Synthetic jets. *Annu. Rev. Fluid Mech.* **34**, 503–529.

IACCARINO, G.,MARONGIU, C., CATALANO, P., AMATO, M. 2003 RANS simulation of the separated flow over a bump with active control. *Annual Research Briefs*, Center for Turbulence Research, NASA Ames/Stanford University.

KRAL, L. D., DONOVAN, J. F., ALAN, B. C. & CARY, A. W. 1997 Numerical simulation of synthetic jet actuators. *AIAA Paper* 1997-1824.

MARONGIU, C., IACCARINO, G., CATALANO, P., AMATO, M. 2004 CASE 3: Investigation of a boundary condition model for the simulation of controlled flows. *CFD Validation Workshop on Synthetic Jets and Turbulent Separation Control.* **1**, March 29-31 Williamsburg, Virginia.

MENTER, F. R. 1994 Two equation eddy viscosity turbulence models for engineering applications. *AIAA J.* **32**, 1598–1605.

MYONG, H., KASAGI, N. 1990 A new approach to the improvement of the $\kappa - \varepsilon$ turbulence model for wall bounded shear flows. *JSME Intern. J.* **33**-1, 63–72.

PES, M., LUKOVIC, B., ORKWIS, P. & TURNER, M. 2002 Modeling of two dimensional synthetic jet unsteadiness using neural network-based deterministic source terms. *AIAA Paper.* 2002-2860.

RILEY, N. 2001 Steady streaming. *Annu. Rev. Fluid Mech.* **33**, 43–65.

RUMSEY, C.L., GATSKI, T.B., SELLERS, W.L., VATSA, S.A., VIKEN, S.A. 2004 Summary of the 2004 CFD validation workshop on synthetic jets and turbulent separation control. *AIAA Paper.* 2004-2217.

SMITH, B.L., SWIFT, G.W. 2003 A comparison between synthetic jets and continuous jets. *Experiments in fluids.* **34**, 467–472.

VIKEN, S. A., VATSA, V. N., RUMSEY, C. L., CARPENTER, M. H. 2003 Flow control analysis of the hump model with RANS tools. *AIAA Paper* 2003-0218.

RUMSEY, C.L., GATSKI, T.B., 2004 CFD validation of synthetic jets and turbulent separation control. *Contributed Papers.* vol. 1-3. http://cfdval2004.larc.nasa.gov/.
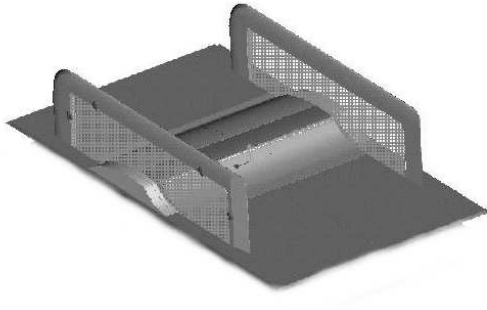
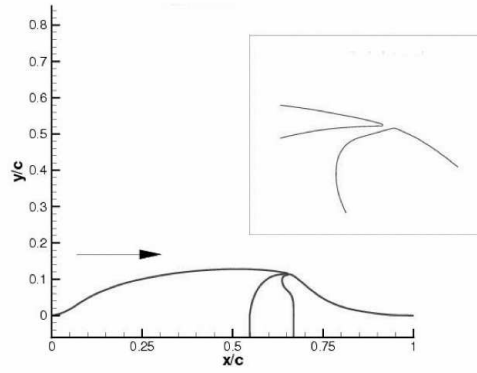FIGURE 1. Hump model experimental set-up.

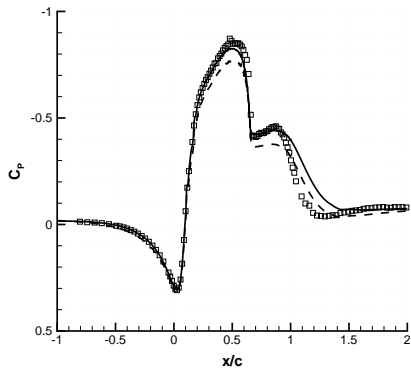FIGURE 2. Hump model: 2D sketch.

FIGURE 3. No control c_p: Exp. (symbol), contoured top wall grid (solid), flat top wall grid (dashed).
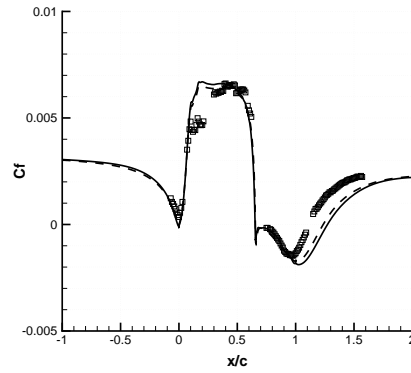

FIGURE 4. No control c_f: Exp. (symbol), contoured top wall grid (solid), flat top wall grid(dashed).
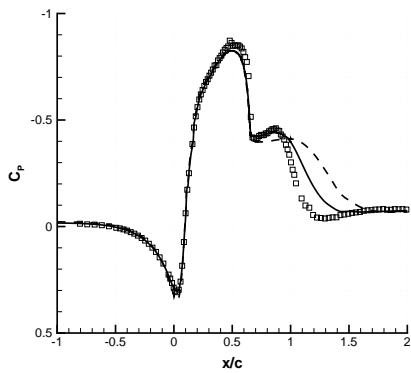

FIGURE 5. No control case c_p: Exp. (symbol), SST $\kappa-\omega$ (solid), $\kappa-\varepsilon$ Myong & Kasagi (dashed).
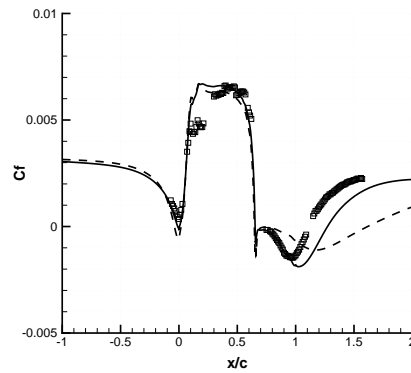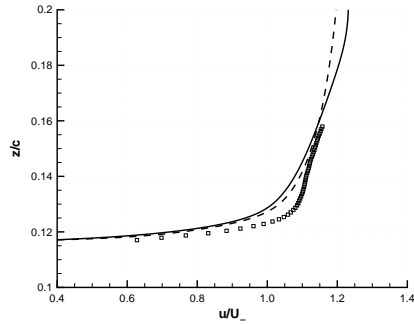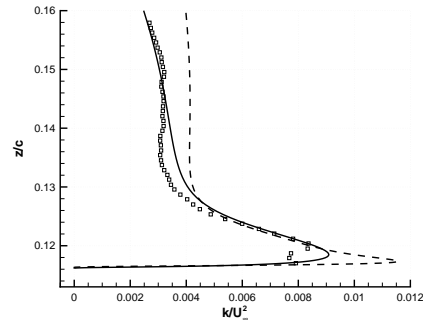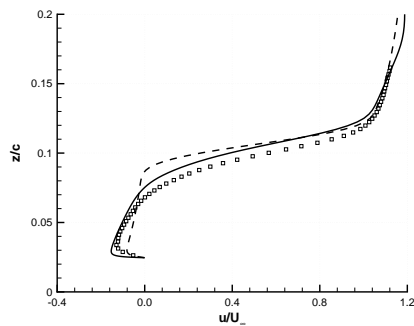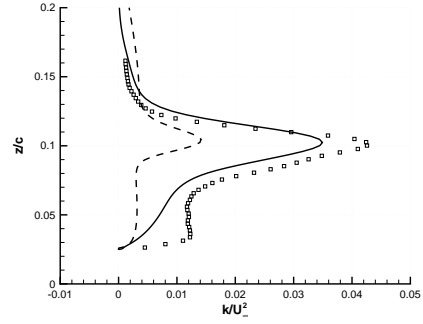

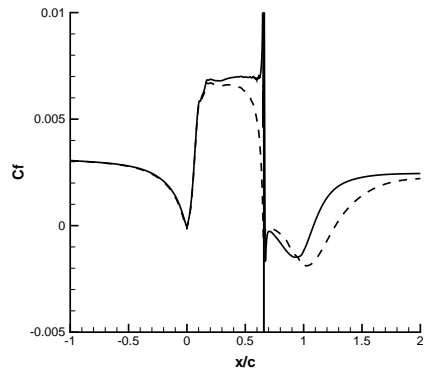FIGURE 6. No control case c_f: Exp. (symbol), SST $\kappa-\omega$ (solid), $\kappa-\varepsilon$ Myong & Kasagi (dashed).
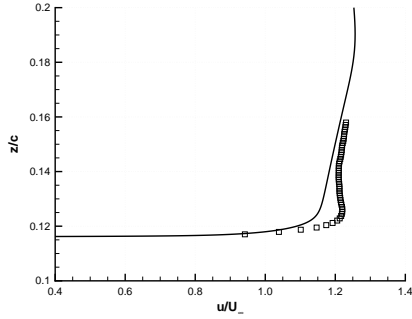
FIGURE 7. No control case: stream-wise velocity at $x/c = 0.65$. Exp. (symbol), SST $\kappa-\omega$ (solid), $\kappa-\varepsilon$ Myong & Kasagi (dashed).

FIGURE 8. No control case: turbulent kinetic energy at $x/c = 0.65$. Exp. (symbol), SST $\kappa-\omega$ (solid), $\kappa-\varepsilon$ Myong & Kasagi (dashed).

FIGURE 9. No control case: stream-wise velocity at $x/c = 0.80$. Exp. (symbol), SST $\kappa-\omega$ (solid), $\kappa-\varepsilon$ Myong & Kasagi (dashed).

FIGURE 10. No control case: turbulent kinetic energy at $x/c = 0.80$. Exp. (symbol), SST $\kappa - \omega$ (solid), $\kappa - \varepsilon$ Myong & Kasagi (dashed).
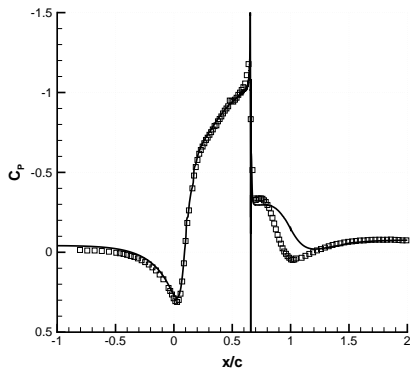
FIGURE 11. Steady suction c_p: Exp. (symbol), SST $\kappa - \omega$ (solid).

FIGURE 12. c_f distribution with SST $\kappa - \omega$: steady suction (solid), baseflow (dashed).

FIGURE 13. Steady suction: stream-wise velocity at $x/c = 0.65$. Exp. (symbol), SST $\kappa-\omega$ (solid), $\kappa-\varepsilon$ Myong & Kasagi (dashed).
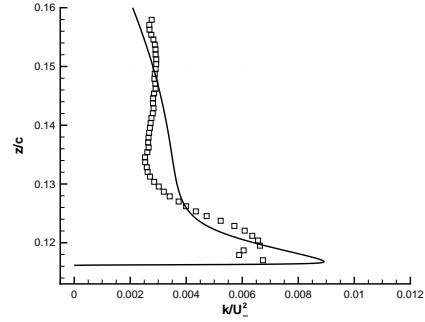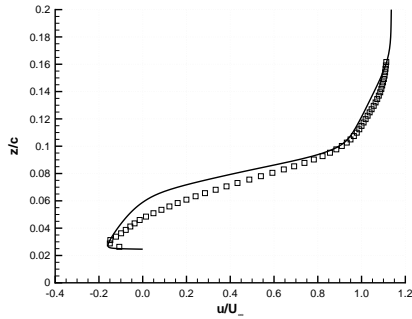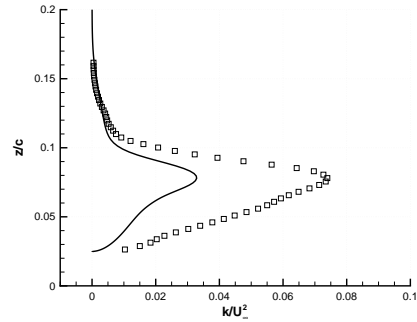

FIGURE 14. Steady suction: turbulent kinetic energy at $x/c = 0.65$. Exp. (symbol), SST $\kappa - \omega$ (solid), $\kappa - \varepsilon$ Myong & Kasagi (dashed).

FIGURE 15. Steady suction: stream-wise velocity at $x/c = 0.80$. Exp. (symbol), SST $\kappa-\omega$ (solid), $\kappa-\varepsilon$ Myong & Kasagi (dashed).

FIGURE 16. Steady suction: turbulent kinetic energy at $x/c = 0.80$. Exp. (symbol), SST $\kappa - \omega$ (solid), $\kappa - \varepsilon$ Myong & Kasagi (dashed).
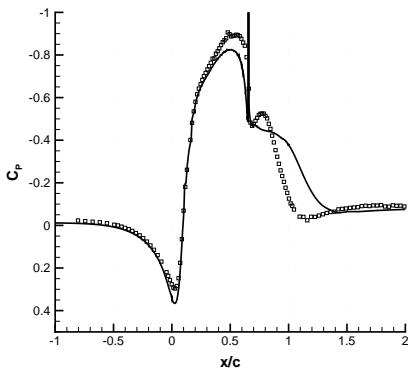

FIGURE 17. Unsteady case; mean c_p: Exp. (symbol), $\kappa - \varepsilon$ Myong & Kasagi(solid).
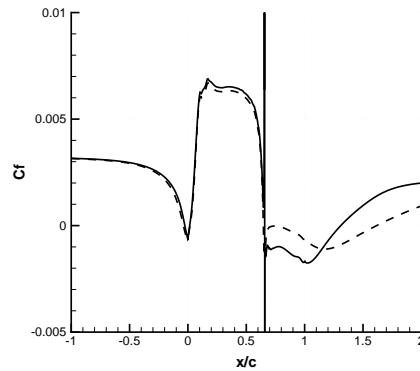

FIGURE 18. Unsteady case; mean c_f: baseflow (dashed), oscillatory control (solid) . $\kappa - \varepsilon$ Myong & Kasagi model.
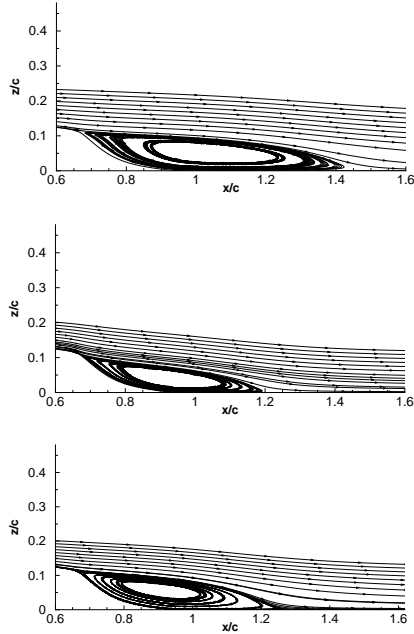
FIGURE 19. Separation bubble: no control (top), steady suction (middle), synthetic jet (bottom). $\kappa - \varepsilon$ Myong & Kasagi.
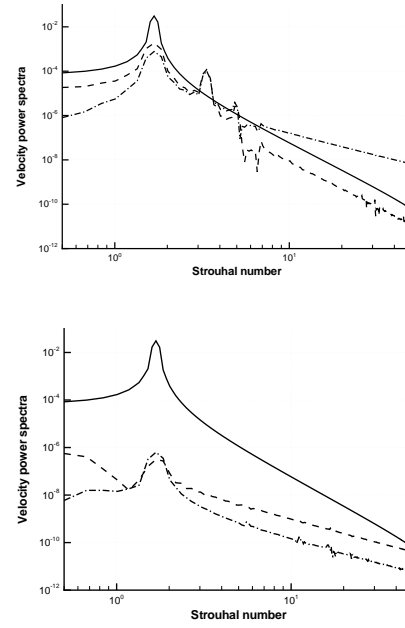

FIGURE 20. Velocity component power spectra in the boundary layer: $x/c = 0.86$ steady bubble zone (top), $x/c = 2.0$ downstream reattachment point (bottom). velocity magnitude (solid), u component (dashed), v component (dash-dot).